Microchimica Acta (2019) 186:592
https://doi.org/10.1007/s00604-019-3701-5

ORIGINAL PAPER

Electrochemical Aflatoxin B1 immunosensor based on the use of graphene quantum dots and gold nanoparticles

Hema Bhardwaj [1,2] · Manoj Kumar Pandey [1] · Rajesh [1] · Gajjala Sumana [1,2]

Received: 24 February 2019 / Accepted: 13 July 2019

Abstract

Electrochemical immunosensor for aflatoxin B1 (AFB1) is described that uses a composite prepared from graphene quantum dots (GQDs) and gold nanoparticles (Au NPs). The GQD-AuNP conjugate was obtained by using 2-aminothiophenol (ATP) as a linker where the carboxy groups of GQD bind to the amino groups of crosslinker via conjugation of thiol binding to the AuNP. To evaluate the conjugation of the GQD-AuNP composite, Fourier transform infrared spectroscopy (FT-IR), and transmission electron microscopy (TEM) was applied. The composite was placed on an indium tin oxide (ITO) electrode and then modified with an antibody against AFB1. By using hexacyanoferrate as the electrochemical probe, the sensor works in the 0.1 to 3.0 ng mL^{-1} AFB1 concentration range, is highly specific, has good reproducibility and acceptable stability. The biosensor was applied to the analysis of (spiked) maize samples. Conceivably, the method can be utilized to sense other mycotoxins by using their respective antibodies.

Keywords Electrophoretic deposition · Food toxin · Cyclic voltammetry · Biosensor · Indium tin oxide

Introduction

A significant amount of, theoretical and experimental studies elucidate the unique structural and electrical properties of graphene with potential application in nanotechnology and nanofabrication area [1]. It is sp^2 hybridized two-dimensional (2-D) material with packed of hexagonal structure. Graphene sheets being considered as the desired material for sensing, imaging, or diagnostic application because of their large surface area, biocompatibility, highly stable, and electrically conductive [2]. However, graphene sheets contain a limited number of edge planes, as well as zero bandgaps that restrict their utilization in many areas [3]. The material characteristic properties can be altered by tuning their structure, which leads to change in several intrinsic properties in the device. The transformation of nanostructure material of 2-D graphene sheets to zero-dimensional (O-D) quantum dots, numerous advantages properties get improved such as electronic, optical, robust chemical inertness, and stabilities. GQDs one of the most attracted nanomaterials for electro-optical devices because of the high surface reactivity, dispersibility, biocompatibility, and wide absorption and narrow emission band spectra that significantly amplify the output signal. GQDs lateral dimension is less than 100 nm along with single, double, or few numbers of layers (i.e., 3–10) where dot size varies to several nanometers [4]. In addition, improvement in the ratio of edge-to-basal planes directly allows the favorable environment for strong bio-nano conjugation in terms of chemical functionalities and reactivity [5]. The existence of this special feature in GQDs remarkably increases the rate of heterogeneous electron transfer, facilitate the conjugation of biomolecules along with dispersion in an aqueous solution that significantly improves the characteristic of biosensors like sensitivity, specificity, and stability.

The noble metal NPs such as gold and silver (Ag), play a vital role in the fabrication of biosensing or bioimaging devices due to their high electrical, optical, and catalytic properties [6]. Au NP is an obvious choice of material that offer

Electronic supplementary material The online version of this article (https://doi.org/10.1007/s00604-019-3701-5) contains supplementary material, which is available to authorized users.

✉ Gajjala Sumana
sumanagajjala@gmail.com

[1] CSIR-National Physical Laboratory, Dr. K.S. Krishnan Marg, New Delhi 110012, India

[2] Academy of Scientific and Innovative Research, CSIR-National Physical Laboratory, Dr. K.S. Krishnan Marg, New Delhi 110012, India

Published online: 01 August 2019

multifold signal enhancement for the construction biosensor due to their non-toxic behaviour, high conductivity, and good catalytic properties. Luo et al. 2006, reported that Au NPs provide a benign environment and attractive analytical behavior that improve multiple times electron transfer rate between electrodes and the active center of biomolecules [7]. These suitable properties provide favorable support to construct precise, accurate, and sensible electrochemical biosensor. Also, it has been reported that structural features, shape, and morphology of the nanomaterials effectively contribute towards the performance of biosensor. From the past few years, the composite of GQDs-AuNPs has paved a great interest in the development of electroanalytical devices due to the combination of interesting properties such as large surface-to-volume ratio and high catalytic activity. Huang et al. 2011, studied the composite of amine-functionalized graphene and Au NPs for direct electrochemistry and electrocatalysis hydrogen peroxide (H_2O_2) sensor [8]. They reported that bioelectrode surface retained their biocatalytic activity, offered fast and sensitive H_2O_2 quantification using the graphene and Au NP. Also, Ju et al. 2015, demonstrated in-situ growth of Au NPs on N-GQDs for electrochemical H_2O_2 detection, and these synthesized nanomaterials deposited on glassy carbon electrode (GCE) using a drop-casting method [9]. Similarly, Li et al. 2016, fabricated an electrochemical sensor for Quercetin detection based on GQDs and AuNPs composite and drop-cast method was applied to deposit the composite GQDs-AuNPs [10]. However, drop-cast method have a lot of limitations including poor uniformity of the film, limited coverage area, leaching of nanomaterials in compared to other technique such as electrophoretic deposition (EPD). EPD is an electrochemical process that used to migrate the colloidal suspended charged particles or molecules/ions toward an electrode surface (cathode or anode) by applying an appropriate electric field in a two-electrode cell. EPD technique has been used to attain a controlled thickness and to obtain a homogenous morphology of the film on electrode surface that play a significant role in obtaining the better electrochemical sensing performance.

Over the last decade, nano-bio sensing techniques have also been considered as an advanced analytical tool for foodborne as mycotoxin detection due to huge agricultural and industrial losses in billions of dollars. Among the various toxins, AFB1 is the most hazardous chemical produced by strains of *Aspergillus flavus* and *Aspergillus parasiticus* fungi species [11]. International Agency for Research on Cancer (IARC) classified AFB1 as a Group-I Human Carcinogen, is responsible for carcinogenic, mutagenic, and immunosuppressive disorders in human beings as well as in animals [12]. The toxicity of AFB1 mainly found in food products such as maize, cereals, groundnuts, pistachio, almond, wheat, etc. Although, there are various conventional techniques available for AFB1 detection such as Thin Layer Chromatography (TLC), High-Performance Liquid Chromatography (HPLC), Gas Chromatography, and Mass Spectroscopy (GC-MS). These techniques have some demerits includes time-consuming, need tedious sample pre-treatment, laborious personnel required as well as expensive equipment. Among these available detection techniques, there is a need of sensitive and selective sophisticated device for reliable and specific detection of AFB1. The electrochemical biosensor is one of the most appropriate, accurate, label-free, reliable techniques to enumerate the toxicity in foodstuff.

In this context, electrochemical label-free immunosensor was fabricated to detect the present AFB1 via antigen-antibodies interactions. Composite of GQDs-AuNPs was prepared by following the chemical method and deposit onto hydrolyzed ITO glass electrode surface using EPD technique. The antibodies of AFB1 were immobilized using N-ethyl-N-(3-dimethylamino propyl) carbodiimide (EDC) and N-hydroxy succinimide (NHS) cross-coupling chemistry. Electrochemical performance of the immunosensor was investigated using Electrochemical Impedance Spectroscopy (EIS) and Cyclic Voltammetry (CV) techniques in a hexacyanoferrate redox probe.

Materials and methods

Reagents and materials

Monoclonal antibodies of AFB1 (anti-AFB1) and respective antigen AFB1 were procured from Sigma-Aldrich (www.sigmaaldrich.com). Sulfuric acid (PubChem CID: 1118, H_2SO_4), nitric acid (PubChem CID: 944, HNO_3), H_2O_2 (PubChem CID: 784, 30%), sodium citrate (PubChem CID: 6224), citric acid (PubChem CID: 311, CA), magnesium nitrate (PubChem CID: 202877, $Mg(NO_3)_2.6H_2O$), EDC (PubChem CID: 2723939), NHS (PubChem CID: 80170,), potassium ferrocyanide (PubChem CID: 129689883, $K_4Fe(CN)_6$), potassium ferricyanide (PubChem CID: 26250, $K_3Fe(CN)_6$), ATP, bovine serum albumin (BSA) purchased from Sigma-Aldrich (www.sigmaaldrich.com), H_2O_2 (PubChem CID: 784, 30% *w/v*) from Thomas Baker (www.thomasbaker.com) and chloroauric acid (PubChem CID: 28133, $HAuCl_4.4H_20$) procured from Molychem (www.molychem.net). The Milli-Q-purified water Millipore (18.2 MΩ cm) was used for the synthesis of nanomaterials and preparation of buffer solutions. All chemicals were of the analytical grade used as such without any further purification.

Instruments

Synthesized GQDs-AuNPs were deposited on ITO coated glass substrate using an EPD technique. Structural, morphological and optical characterization were carried out using

spectroscopy, diffractometry, microscopic techniques such as UV-visible spectroscopy (Lambda 950, PerkinElmer), Photoluminescence spectroscopy (PL, Jobin Yvon-Horiba, Model 3–11), X-ray diffractometry (XRD, Cu Kα radiation, Rigaku), FT-IR (Spectrum BX, Perkin Elmer), TEM (Technaii-G2F30 STWIN), Scanning electron microscopy (SEM, LEO 440) equipped with Energy-dispersive X-ray (EDX) spectroscopy. Confocal fluorescence microscopic analysis was carried out by an Olympus IX51 inverted system. Electrochemical studies were carried out using CV and EIS (Autolab Galvanostat/Potentiostat Eco Chemie, the Netherlands, model AUT 84275) in phosphate buffer saline (PBS, 50 mM containing 0.9% NaCl, pH 7.4) having 5 mM $[Fe(CN)_6]^{3-/4-}$ using as a redox probe in three-electrode cell containing working electrode (ITO), counter electrode (Pt) as well as reference electrode (Ag/AgCl).

Synthesis of gold nanoparticles

Au NPs was synthesized using a previously reported method with slight modifications [13]. In a 100 mL of the conical flask, 50 mL of $HAuCl_4.4H_20$ solution (0.25 mM) was taken and kept on a heating mantle was brought to boiling. Under mild stirring, 1% of sodium citrate was added. Sodium citrate initially acts as a reducing agent after that capped on the Au NPs to prevent the agglomeration. During the reaction period, the color of the mixture changed from pale yellow to colorless then to blue and finally to ruby red. After that conical flask removed from the magnetic stirrer and cools down at room temperature. Kept it in a refrigerator 4 °C by covering with foil paper.

Synthesis of graphene quantum dots and its composite with gold nanoparticles

GQDs was synthesized by pyrolysis reduction method using CA as a precursor [14]. In a typical, 2 g of CA was taken in 5 mL of the beaker and heated to 200 °C on a heating mantle. After 5 minute, CA was liquated, and after 30 minute, the color of the reaction mixture was changed from colorless to pale yellow then to orange indicate the formation of GQDs. After that, 100 mL of 10 mg mL^{-1} sodium hydroxide (NaOH) was added drop by drop in the above solution under vigorous stirring, and an aqueous solution of GQDs was obtained. Further, the composite of GQDs and AuNPs was synthesized by the chemical conjugation. Briefly, in a 10 mL of the beaker, an aqueous solution of GQDs (0.5 mg mL^{-1}) and Au NPs (2 mL) was taken, and ATP (0.25 mg) was added into the above reaction mixture which was used as a crosslinker and kept on stirring for 3 hour at 30 °C. The yellowish-red color of GQDs-AuNPs was obtained. Finally, the suspension was ultracentrifuged at 5000 rpm followed by washing with distilled water two times to remove the impurities.

Electrophoretic deposition of composite GQDs-AuNPs

Figure 1 illustrates the synthesis of composite GQDs-AuNPs followed by transfer of composite on the electrode surface, and fabrication of electrochemical immunosensor for AFB1 detection. The synthesized colloidal suspension of composite GQDs-AuNPs was deposited on the ITO electrode substrate using EPD technique. Before to carried out EPD process, ITO coated glass substrate was hydrolyzed by dipped them into a solution mixture of $H_2O_2/NH_3/H_2O$ (1:1:5 *v/v*) and kept in the oven for half an hour at 80 °C then dried at room temperature. Synthesized composite GQDs-AuNPs (1000 μL) were dispersed in distilled water (10 mL) and $Mg(NO_3)_2.6H_2O$ (10^{-5}–10^{-4} M) was added as an electrolyte further sonicated for 20 minute. For the deposition process, the colloidal suspension was taken into two-electrode cells separated by 1 cm, and the DC potential of 10 V was applied for 30 second. Due to the presence of a positive charge in colloidal suspension, composite migrated towards the ITO electrode surface under the applied potential. After that electrode was removed from the suspension rinsed with distilled water and dried at room temperature.

Fabrication of bioelectrodes using antibody of aflatoxin B1

Before to carried out the immobilization process, electrodes were treated with EDC-NHS crosslinker to activate the functional groups of a composite. Crosslinker EDC (0.2 M) act as a coupling agent and NHS (0.05 M) act as an activator [15]. 50 μL of EDC-NHS was dispersed over the surface of the electrode of GQDs/ITO, and GQDs-AuNPs/ITO kept under the humid condition at room temperature for 4 hour. After that, 50 μL of anti-AFB1 (10 μg mL^{-1}) was dispersed over electrodes surface and kept in a humid chamber for 12 hour at 25 °C. Finally, electrodes were treated with 1% of BSA to block nonspecific adsorption sites and stored it in a refrigerator 4 °C for further use.

Preparation of real sample

Uncontaminated maize samples purchased from the local market was used for the real sample analysis against faricated immunosensor. For sample preparation, 1 g of maize sample weighed and spiked with AFB1 concentration. After that, 5 mL of ethanol (80% *v/v*) was added and shake on a vortex shaker for 45 minute [16]. Various concentration of the solution was obtained by diluted with phosphate buffer and tested against fabricated bioelectrode of anti-AFB1/GQDs-AuNPs/ITO in 50 mM of PBS containing 5 mM of $[Fe(CN)_6]^{3-/4-}$ using CV technique (Fig. 1).

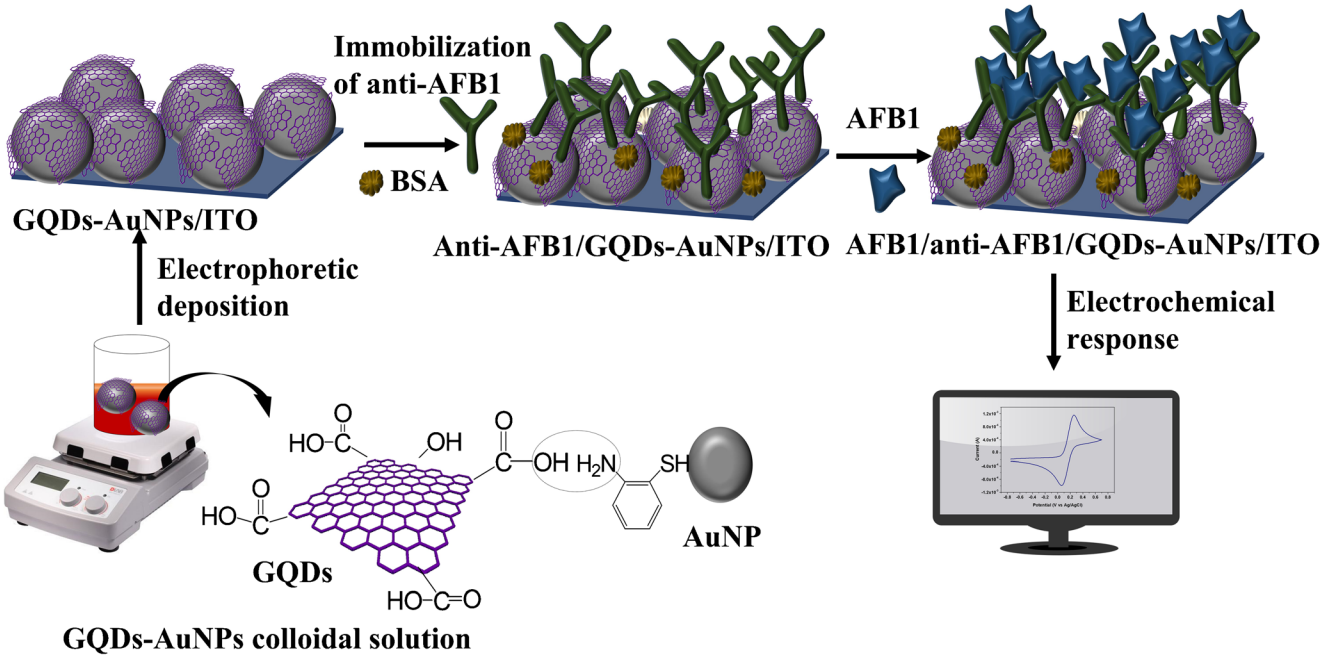

Fig. 1 Schematic representation of the synthesis of composite graphene quantum dots-gold nanoparticles (GQDs-AuNPs) and Electrophoretic Deposition (EPD) of synthesized composite onto ITO electrode and fabrication of anti-AFB1/GQDs-AuNPs/ITO bioelectrode for Aflatoxin B1 detection

Results and discussion

Optical studies

The UV-visible spectrum of synthesized GQDs, Au NPs, and composite of GQDs-AuNPs is shown in Fig. 2 (a-b). As seen from the Fig. 2 curve (a) of AuNPs, the peak appeared at 525 nm attributed to surface plasmon resonance absorption band indicates the formation of Au NPs [17]. The UV-visible spectrum of GQDs shown in inset image of Fig. 2. The broad absorption peak appeared at 320 nm due to n-π* electronic transition, which corresponds to aromatic sp^2 domains behaviour. This study indicates that functional groups of moieties are present in the structure of GQDs [18]. The UV-visible spectrum of composite GQDs-AuNPs is shown in Fig. 2 curve (b), two absorption peaks appear at 528 nm, and 312 nm indicates the formation of composite GQDs-AuNPs. However, the absorption peak of Au NPs and GQDs are slightly shifted towards the higher wavelength from 525 nm to 528 nm and a lower wavelength from 320 nm to 312 nm respectively, indicates the binding of GQDs to Au NPs.

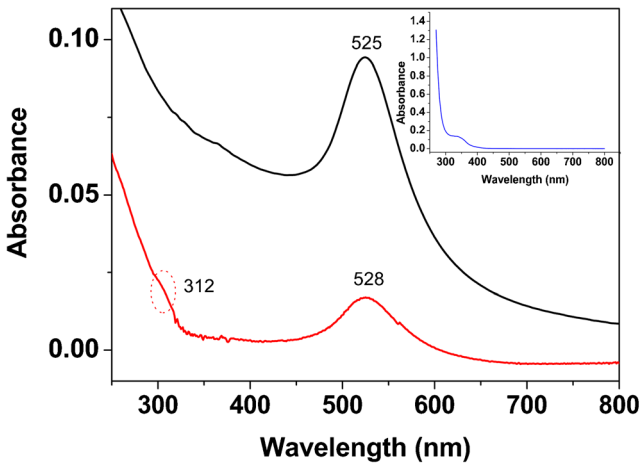

Fig. 2 UV-visible spectrum of **(a)** Gold nanoparticles (Au NPs), **(b)** composite of GQDs-AuNPs [inset image: represents UV-visible spectrum of GQDs]

PL Spectroscopy study of GQDs aqueous solution under the excitation of wavelength at 320 nm was carried out. Fig. S1 (a) shows PL emission spectrum, the peak appeared at 420 nm wavelength due to polyaromatic sp^2 carbon nanostructure as well as the various edge and surface functional groups [19].

X-ray diffraction studies

XRD technique was utilized to investigate the purity and crystallinity of the synthesized nanomaterial. As shown in Fig. S1(b) curve (a), a narrow diffraction peak appeared at 23.6° found to be lower than graphite diffraction peak ($d_{002} = 25°$) indicates the formation of GQDs. Further, synthesized AuNPs have also been characterized, and the results are shown in curve (b). Several diffraction peaks appeared at 38°, 45°, 64.3°, 76.9° corresponds to (111) ($d_{111} = 2.36A°$), (200) ($d_{200} = 2.05A°$), (220), (311) planes attributed to face-centered cubic (FCC) structure [JCPDS 89–3697] [20]. Also, XRD diffraction pattern of synthesized composite GQDs-AuNPs depicts in the curve (c) where characteristic

diffraction peaks are appeared along with the difference in the peak intensity. The primary diffraction peak of GQDs appeared at 23.6° due to 002 plane. Moreover, several diffraction peaks appeared at 38°, 64.3°, 76.9° corresponds to AuNPs and rest of the peak appeared at 30.5°, 31.8°, 35.1°, 50.8°, 60.0° due to ITO surface [JCPDS 89–4596] [20].

Spectroscopic analysis

FT-IR studies were carried out to determine the present functional groups in nanomaterials (GQDs/ITO, GQDs-AuNPs/ITO) as well as conjugated biomolecules (anti-AFB1/GQDs-AuNPs/ITO). Figure 3(a) shows the FT-IR spectrum of GQDs/ITO electrode, a broad peak appeared at 3500 cm^{-1} corresponds to hydroxyl (-OH) groups of carboxylic acid and other peaks appeared at 1650 1400, 845 cm^{-1} attributed to -C=O, -C=C, aromatic C-H bending groups in GQDs, respectively. Moreover, FT-IR spectrum of composite GQDs-AuNPs is shown in Fig. 3(b), the peak appeared at 3463 cm^{-1} attributed to amide bond formation between GQDs-AuNPs through crosslinker. Also, characteristic peaks appeared at 2814, 1600, and 1385 cm^{-1} indicates the formation of thiolate bonds, amide bonds, and amine bonding in the composites, respectively. This amide bond is appeared because of the ATP groups which act as a crosslinker for binding of GQDs to AuNPs. Further, FT-IR spectrum of anti-AFB1/GQDs-AuNPs/ITO has also been taken and shown in Fig. 3(c). In addition to above-mentioned peaks, some additional peaks appeared at 3568, and 1492 cm^{-1} corresponds to N-H stretching bond amide bond (II) formation, respectively [21]. These peaks confirmed the covalent linkage occurred between biomolecules with GQDs-AuNPs electrode surface.

Microscopic studies

TEM technique was utilized to determine the shape and size of NPs. Dispersed colloidal solutions of GQDs, AuNPs, and GQDs-AuNPs composite was prepared in distilled water and drop-cast onto carbon-coated copper grids (3.05 mm). TEM images of GQDs are depicted in Fig. 4(a, b) shows synthesized GQDs are spherical and monodispersed. The average size in diameter of GQDs is 6–8 nm. TEM images of AuNPs are shown in Fig. 4(c, d) illustrates that Au NPs well-dispersed as well as uniformly distributed. The average size of the AuNPs lies in the range of 15 to 20 nm. Moreover, the atomic scale in selected area electron diffraction (SAED) pattern is shown in inset image 4(d), and the interplanar lattice fringes found to be 0.23 nm which corresponds to (111) diffraction plane. Figure 4(e, f) depicts the TEM images of composite GQDs-AuNPs, which confirmed the conjugation of GQDs and AuNPs. Lattice fringes of the composite found to be 0.33 nm and 0.23 nm.

Morphology studies

SEM studies were carried out to determine the surface morphology of nanocrystals (GQDs and GQDs-AuNPs) on ITO surface as well as immobilized biomolecules of anti-AFB1 on GQDs-AuNPs/ITO surface and acquired images is depicted in Fig. S2(a-d). The GQDs nanocrystals were deposit electrophoretic by applying a small amount of voltage to obtain well-ordered distribution over the electrode surface [Fig. S2(a)]. It is found that nanocrystals (GQDs) uniformly deposited over ITO electrode surface with an even morphology along with the appearance of small grains. Moreover, SEM

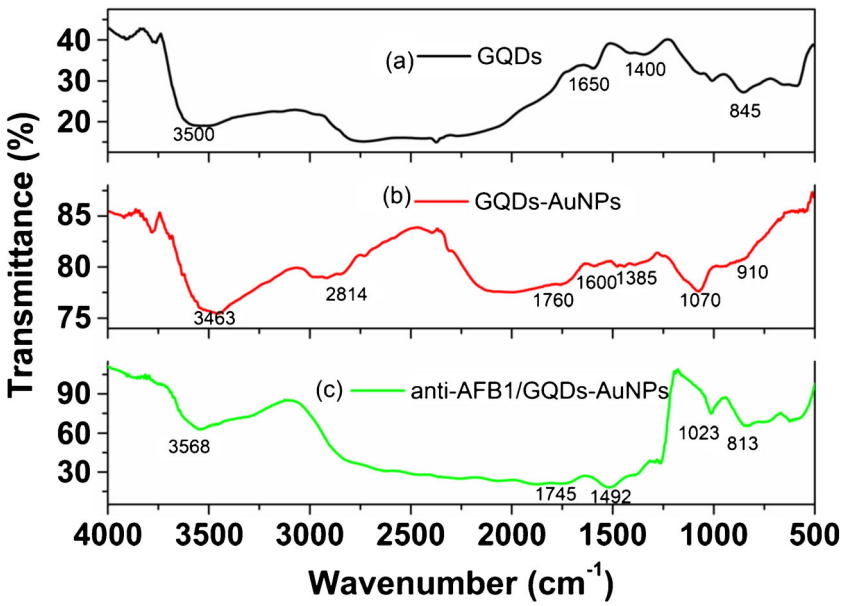

Fig. 3 Fourier Transform Infrared spectrum (FT-IR) of **(a)** GQDs/ITO, **(b)** nanocomposite GQDs-AuNPs/ITO, **(c)** antibody immobilized on composite GQDs-AuNPs/ITO electrode

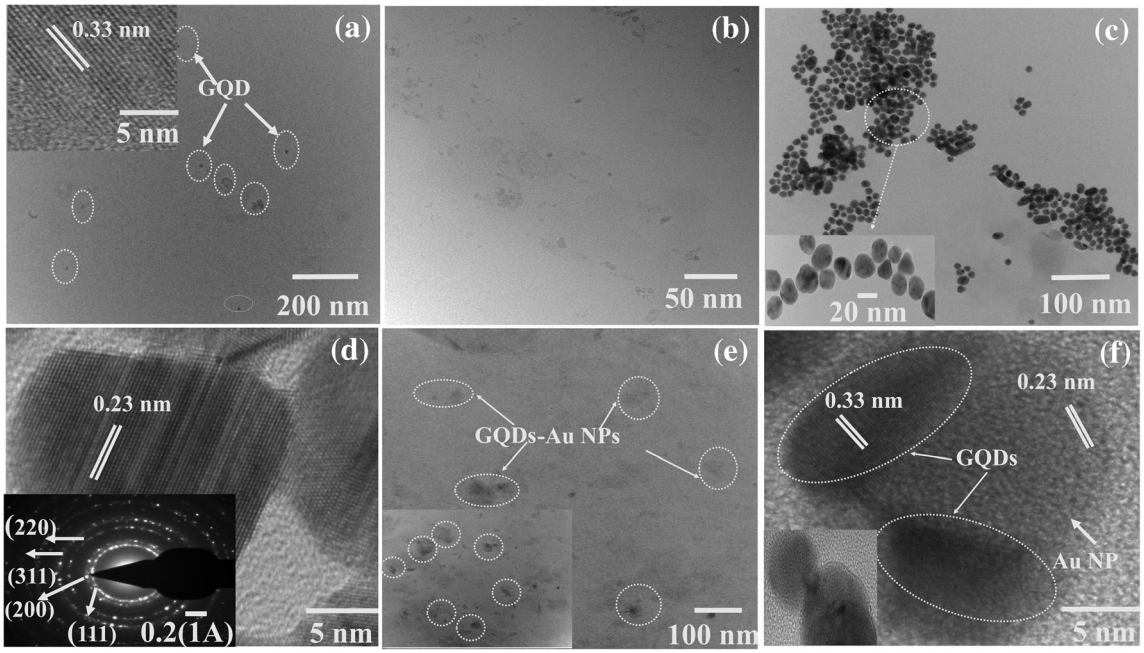

Fig. 4 Transmission Electron Microscopy (TEM) images **(a-b)** of GQDs (inset image: showing lattice fringes), **(c-d)** of AuNPs (inset image: showing the selected area electron diffraction (SEAD pattern)) and **(e-f)** composites of GQDs-AuNPs with lattice fringes

image of nanocrystals GQDs-AuNPs acquired and micrograph is shown in Fig. S2(b), revealed the uniform deposition of a composite over the ITO electrode surface. It can be seen that the surface morphology of the composite nanocrystals electrode (GQDs-AuNPs) is different from the nanocrystals electrode (GQDs) in terms of the distribution of particles and the appearance of grains. Furethermore, immobilization of biomolecules of anti-AFB1 on GQDs-AuNPs/ITO electrode also confirmed by SEM technique and images is shown in Fig. S2(c). The appearance of the globular structure along with uniform coverage confirmed the successful immobilization of biomolecules on the electrode surface. Further, elemental analysis was carried out using EDX spectroscopy, and results are depicted in Fig. S2(d). The presence of elemental composition of anti-AFB1/GQDs-AuNPs/ITO fabricated electrode surface was confirmed by EDX analysis. EDX spectrum, shown in Fig. S2(d), contains carbon, Au, oxygen of the composite GQDs-AuNPs and biomolecules while the presence of some ions such as sodium, magnesium, sulphur elements attributed to biomolecule ions. Moreover, the appearance of indium element is due to the ITO electrode surface. It can be concluded from the above result that nano-bio interface region is successfully formed.

Before performing the electrochemical experiments with immobilized antibodies anti-AFB1/GQDs-AuNPs/ITO electrodes, presence of antibodies on the fabricated surface was confirmed by the confocal fluorescent imaging technique. Fluorescence imaging studies were carried out by immobilizing the primary antibody (Ab-AFB1) and Fluorescein isothiocyanate (FITC) tagged monoclonal antibody as secondary antibody onto the GQDs-AuNPs/ITO surface. The fluorescence images were recorded using a confocal fluorescence microscope and results are shown in Fig. S3. These FITC-tagged secondary antibody absorb UV light in the range of 470 to 490 nm to excite the molecules correspondingly emit a visible yellow or green light. The appearance of bright dark green color after the immobilization signifies that antobodies of AFB1 successlfully attached with GQDs-AuNPs/ITO surface.

Electrochemical studies

Electrochemical characterization studies were carried out for GQDs/ITO, GQDs-AuNPs/ITO, and anti-AFB1/GQDs-AuNPs/ITO electrodes using the electrochemical technique such as CV and EIS technique.

In a three-electrode system, CV studies were carried out to measure the interaction between biomolecules and the solid surface under Potentiodynamic conditions which record current response while the potential scan is applied to the working electrode at a constant scan rate. CV studies were performed for GQDs/ITO, GQDs-AuNPs/ITO, anti-AFB1/GQDs-AuNPs/ITO, BSA/anti-AFB1/GQDs-AuNPs/ITO electrodes at 50 mV s^{-1} in 50 mM PBS (0.9% NaCl) containing 5 mM $[Fe(CN)_6]^{3-/4-}$ pH 7.4 redox probe [Fig. 5(a)]. The anodic and cathodic peak current response of GQDs/ITO electrode found to be 5.0×10^{-4}A and -4.3×10^{-4}A, for GQDs-AuNPs/ITO electrode found to be 1.1×10^{-3}A and -9.8×10^{-4}A whereas for immobilized electrodes anti-AFB1/GQDs-AuNPs/ITO and BSA/anti-AFB1/GQDs-AuNPs/ITO anodic peak current found to be 8.1×10^{-4}A and 7.3×10^{-4}A respectively.

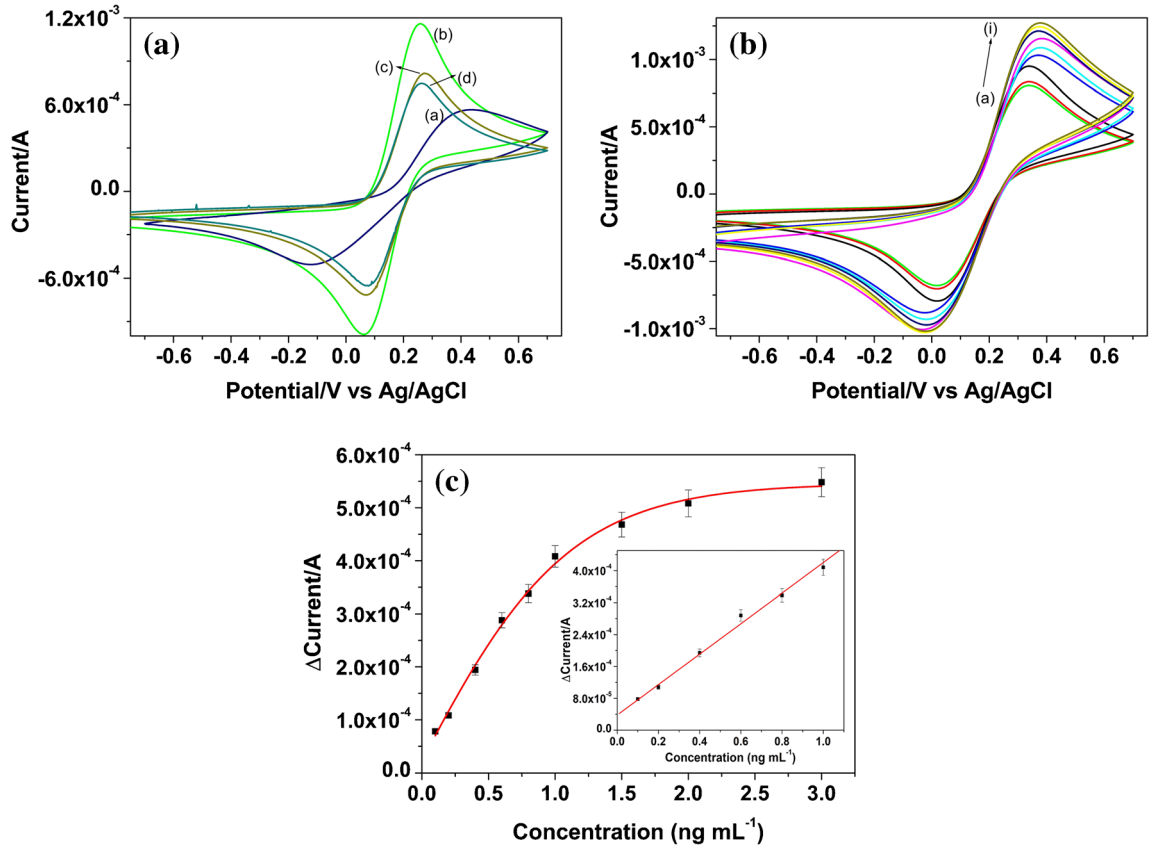

Fig. 5 **(a)** Cyclic Voltammetry (CV) studies of (a) GQDs/ITO, (b) GQDs-AuNPs/ITO, (c) anti-AFB1/GQDs-AuNPs/ITO, (d) BSA/anti-AFB1/GQDs-AuNPs/ITO, **(b)** Cyclic voltammetry response of BSA/anti-AFB1/GQDs-AuNPs/ITO as a function of antigen (0.1–3.0 ng mL^{-1} as 0.1, 0.2, 0.4, 0.6, 0.8, 1.0, 1.5, 2.0, 3.0 ng mL^{-1}) and **(c)** Calibration curve plot of current response as a function of antigen concentration AFB1 (0.1, 0.2, 0.4, 0.6, 0.8, 1.0, 1.5, 2.0, 3.0 ng mL^{-1}) [inset image: linear plot of current response as a function of antigen AFB1 concentration 0.1, 0.2, 0.4, 0.6, 0.8, 1.0 ng mL^{-1}]

Relative to the GQDs electrode surface, electrocatalytic activity of AuNPs correspondingly improves an electronic as well as optical properties of the composite GQDs-AuNPs. The current response of GQDs-AuNPs composite in terms of oxidation and reduction peak significantly enhanced may be due to the existence of the synergistic effect between GQDs and AuNPs. However, in the case of biomolecules meant after immobilization of anti-AFB1 on GQDs-AuNPs electrode surface, current response found to be decreased because of higher loading of an antibody that creates a hindrance in transferring the electrons between electrodes and electrolyte system. Further, the current response significantly decreased after the interaction with BSA, which blocks non-active available sites over the electrode surface [22]. The electrochemical scan rate study of BSA/anti-AFB_1/GQDs-AuNPs/ITO bioelectrode was also investigated by CV technique at various scan rate from 10 mV s^{-1} to 100 mV s^{-1} [Fig. S4]. The anodic and cathodic peak current value (I_{pa} and I_{pc}) and potential peak values (E_{ap} and E_{cp}) found to increased towards the positive as well as negative direction as by varying the scan rate, indicating good electrochemical reaction ability and fast electron transfer kinetics. Fig. S4 inset image shows the redox current response which found to vary proportionally with the square root of the scan rate, specifies the quasi-reversible diffusion-controlled process [23]. The anodic and cathodic peak current values are shown in eqs. (1–2),

$$I_{ac} = 7.190x10^{-5}\,A + 1.22x10^{-4}\left(A^2\,m\,V^{-1}\,s\right)^{1/2} \times\left[scan\ rate\left(mV\,s^{-1}\right)\right]^{1/2}; R^2 = 0.99 \quad (1)$$

$$I_{cc} = -1.923x10^{-4}A - 8.3079x10^{-4}\left(A^2\,m\,V^{-1}\,s\right)^{1/2} \times\left[scan\ rate\left(mV\,s^{-1}\right)\right]^{1/2}; R^2 = 0.99 \quad (2)$$

According to the Randles-Sevcik equation, the intensity of peak current mainly depends upon the two factors, i.e., the surface area of the working electrode and secondly, on the concentration of electro-active species. The diffusion coefficient (D) of the electrode and bioelectrodes was calculated using the Randles-Sevcik eq. (3) [24].

$$I_P = 2.69x10^5 n^{3/2} A D^{1/2} V^{1/2} C \quad (3)$$

Where Ip is the peak current (A), n is the no. of electrons, C is the concentration of redox species (5 mM), D is the diffusion coefficient, A is the area of the electrode, and V is the scan rate (50 mV s^{-1}). The D value found to be 5.3x10^{-5} cm^2 s^{-1} for GQDs-AuNPs, 4.12 × 10^{-5} cm^2 s^{-1} for anti-AFB1/GQDs-AuNPs/ITO and 3.7 × 10^{-5} cm^2 s^{-1} for BSA/anti-AFB1/GQDs-AuNPs/ITO electrode. The surface concentration of the GQDs/ITO, GQDs-AuNP/ITO electrodes and anti-AFB1/GQDs-AuNPs/ITO bioelectrode was determined using Brown-Anson model eq. (4) [20],

$$I_P = n^2 F^2 I^* A v / 4RT \quad (4)$$

Where, n is the number of electrons transferred (1), F is the Faraday constant (96,584 C mol^{-1}), I* the surface concentration of films (mol cm^{-2}), A is the surface area of electrode, V is the scan rate (50 mV s^{-1}), R is the gas constant (8.314 J/(mol K)), and T is the absolute temperature (298 K). The surface concentration of the electrode GQDs-AuNPs (4.6 × 10^{-8} mol cm^{-2}) found to be higher than GQDs (2.12 × 10^{-8} mol cm^{-2}). This increment indicates electroactive surface area increases due to the composite of GQDs-AuNPs matrix. However, the surface concentration of the bioelectrode found to be 4.0 × 10^{-8} mol cm^{-2}.

Electrochemical impedance spectroscopy studies

EIS technique is the powerful diagnostic tool to execute the resistive, capacitive, and inductive behavior of the three-electrode cell at a particular frequency. Frequency response analyzer (FRA) is used to impose a small amplitude of AC signal as a function of frequency 0.01–10^5 Hz at bias potential 0.25 V. This technique used for the determination of biomolecules interaction, adsorption behavior, interfacial properties between the electrode and the electrolyte using Randel's equivalent circuit possess solution phase resistance (R_s), capacitance of double layer (C_{dl}), charge transfer resistance (R_{CT}) and Warburg diffusion element (W) from bulk solution to the electrode surface [25]. EIS spectrum of the (a) GQDs/ITO, (b) GQDs-AuNPs/ITO, (c) anti-AFB1/GQDs-AuNPs/ITO, (d) BSA/anti-AFB1/GQDs-AuNPs/ITO electrodes depicted in Fig. S5, experiments were carried out in 50 mM PBS (pH 7.4, 0.9% NaCl) containing 5 mM $[Fe(CN)_6]^{3-/4-}$. It is observed that R_{CT} value for (b) GQDs-AuNPs/ITO electrode found to be 201.8 Ω, after the immobilization of antibody on electrode (c) anti-AFB1/GQDs-AuNPs/ITO, R_{CT} value found to be increased 506 Ω because of the higher loading of biomolecules over the electrode surface which enhanced charge transfer resistance between the interfacial layer of electrode/electrolyte. Moreover, R_{CT} value further increased up to 532 Ω after the treatment with BSA, which block their non-active sites on the electrode surface. Here, R_{CT} value of the (b) GQDs-AuNPs/ITO found to be low (201.8 Ω) as compared to (a) GQDs/ITO (297.94 Ω) electrode because of GQDs-AuNPs composite served as a mediator for electron transport between electrode surface and bulk solution containing redox probe $[Fe(CN)_6]^{3-/4-}$. Hence, these results signify that electron tunneling distance get reduced which leads to enhance electron transfer process.

Heterogeneous Electron Transfer kinetics of the redox probe occurred at the electrode and electrolyte interface which vary accordingly with the modification of the electrode surface. Any insulating modification such as biomolecules expected to retard the electron transfer process through increasing the resistance in charge transfer value. The change in heterogeneous electron transfer value indicates the speed of electron exchange between the electrochemical redox probe $[Fe(CN)_6]^{3-/4-}$ and the electrode surface. Heterogeneous electron transfer for GQDs-AuNPs/ITO electrode and BSA/anti-AFB_1/GQD-AuNPs/ITO bioelectrode was calculated using eq. (5) [26],

$$K_e = \frac{RT}{n^2 F^2 A R_{CT} C} \quad (5)$$

Where, R is the gas constant (8.314 J mol^{-1} K^{-1}), T is the temperature (298 K), n is the no. of the electron transfer constant of the redox couple ($n = 1$), F is the Faraday constant (96485.3 C mol^{-1}), A is the effective area of the electrode (cm^2), R_{CT} is the charge transfer resistance (Ω), C is the concentration of redox species (5 mM). The Ke value of the GQDs-AuNPs/ITO electrode found to be 5 × 10^{-5} cm $s^{-1,}$ whereas the Ke value of BSA/anti-AFB1/GQDs-AuNPs/ITO electrode found to be 2.0 × 10^{-5} cm s^{-1}. The lower Ke value for immobilized antibody as compared to material electrode probably due to heavier bulky groups present in the structure of antibody, which creates hindrance in transferring the electrons. Moreover, the surface coverage of antibodies over the GQDs-AuNPs/ITO electrode estimated by using the relationship of Eq. (6),

$$\theta = 1 - \frac{R_{CT(electrode)}}{R_CT_{(electrode+bioelectrode)}} \quad (6)$$

Here, θ is the fraction of occupied binding sites and R_{CT} of electrode and bioelectrode are the charge transfer resistance before and after the immobilization of antibodies. The value of surface coverage found to be 0.62, indicating more than 60% surface coverage of GQDs-AuNPs/ITO by antibodies of AFB1.

Electrochemical response studies

CV studies were carried out to examine sensing response of BSA/anti-AFB1/GQD-AuNPs/ITO bioelectrode with varying

the concentration of AFB1 from 0.1 to 3.0 ng mL^{-1} in a redox probe containing 50 mM PBS (pH 7.4, 0.9%NaCl) having 5 mM $[Fe(CN)_6]^{3-/4-}$ redox species [Fig. 5(b, c)]. It is observed that the current response in terms of the anodic peak of BSA/anti-AFB_1/GQD-AuNPs/ITO bioelectrode increases proportionally by increasing the analyte concentration from 0.1 to 1.0 ng mL^{-1}. This signal improvement mentioned here is most likely due to the interaction that occurred between AFB1 and anti-AFB1 specifically on the surface platform of GQDs-AuNPs layer.

During the formation of immunocomplex between antigen and antibodies, current response increases, which can be explained by some causing factor such as the formation of the electron transfer layer and the occurrence of changes in conformational structure. For example, Sharma et al. 2015, reported that the magnitude of the current response increases as in addition to analyte concentration revealed the formation of the electron transfer layer [27]. Moreover, Okuno et al. 2007, reported that the current response of immunoelectrode increases as by increasing the concentration of antigen because of the conformational changes occurred during the binding process, this change may permit the transfer of electron more readily through the electrolyte [28]. However, these findings of results revealed that GQDs-AuNPs based platform improve conducting path between redox couples and sensing electrode [29]. Hence, the composite of GQDs-AuNPs played an important role in enhancing the current response as a function of the concentration of AFB1 due to the facile charge transfer accelerating layer. Calibration plot of the bioelectrode depicts in Fig. 5(c), inset image indicates the linear variation of anodic peak current with analyte concentration from 0.1 to 1.0 ng mL^{-1}. After that, on further addition of AFB1 concentration, the little increment is observed in the current signal indicates the interaction of AFB1 antibody and antigen on the electrode surface.

$$I_p = 3.8052 \times 10^{-5}(A) + 3.8210 \times 10^{-4}\left(Ang^{-1}mL\right) \times \text{Concentration}\left(ngmL^{-1}\right) \text{Regression coefficient } \left(R^2\right) = 0.99 \quad (7)$$

The sensitivity of immunosensor and limit of detection found to be 382 μA/ng mL^{-1}/cm^2 and 0.008 ng mL^{-1}. The limit of detection was calculated using the expression ($3\sigma/m$) where m is the slope of the calibration plot, and σ is the standard deviation (S N^{-1} = 3). These findings of improved sensitivity and limit of detection probably due to the composite of GQDs-AuNPs that enhanced electrochemical properties of the immunosensor. Improved surface-to-volume ratio provides more surface area for a large number of biomolecules attachment over the nanomaterials electrode surface; thereby, it modifies the redox conversion probe during the reaction. Composite of GQDs-AuNPs is also increase the conductivity path by increasing the electron transfer signal as compared to the GQDs alone. Ju et al. 2015, studied the Au-GQDs matrix for H_2O_2 detection resulted in the better electrochemical performance of sensor [9]. Moreover, Li et al. 2016, reported that the composite of GQDs/AuNPs involves fast electron transfer capacity and attained high electrochemical activity, which acts as a promising candidate for electrochemical sensing performance [10]. The obtained sensing results from the designed immunosensor have been reported in the Table 1 [30–35], in comparison to other reported work for the detection of a small molecule as AFB1.

Intriguingly, three causative factors mainly matter for better electrochemical activity of immunosensor integrated nanostructured materials such as accelerating the electron transfer rate, enlarging the surface area, and improving nano-bio conjugation for the target analyte. In addition, improved surface-to-volume ratio, present large number of functional groups, remarkably enhance interfacial properties, decrease electron transportation distance, and diffusion length implies to acehive better performance of biosensor for AFB1 detection.

Optimization of antibody aflatoxin B1

The concentration of antibody plays an important role in influencing the sensitivity of the immunosensor. The optimum concentration of anti-AFB1 for this study was examined by CV technique. The different concentration of anti-AFB1 (1–20 μg mL^{-1}) was immobilized, and study was carried out in 50 mM PBS containing (0.9% NaCl) 5 mM $[Fe(CN)_6]^{3-/4-}$ using the same protocol as mentioned in the earlier 'Fabrication of bioelectrodes using antibody of Aflatoxin B1' section. The current response is increased up to the concentration of antibody 10 μg mL^{-1} after that insignificant changes is observed [Fig. S6]. This may be ascribed to the molecular bonding between antibody and composite, which gets saturated at 10 μg mL^{-1} concentration of anti-AFB1.

Real sample analysis

To validate the performance of fabricated biosensor, analysis with real samples is one of the important aspects. Non-contaminated maize samples were used, and various spiked concentrations of AFB1 were examined against fabricated bioelectrode anti-AFB1/GQDs-AuNPs/ITO using CV technique, and results depicted in Fig. S8(a-b). It is observed that current signal increases as by increasing the concentration of AFB1 from 0.1 ng mL^{-1} (0.32 nM) to 2.5 ng mL^{-1} (8 nM) and regression coefficient found to be 0.99 revealed high degree of dependence of current signal to concentration variable. Therefore, this study demonstrating that fabricated immunosensor can be utilized for AFB1 detection in the analysis of maize samples.

Table 1 the comparative studies of reported immunosensor for Aflatoxin B1 detection with present work

S.No.	Bioelectrode	Technique	Detection limit (ng/mL)	Detection range (ng/mL)	sensitivity	References
1.	PTH[a]/Au/GCE[b]	[h]DPV	0.07	0.6–2.4	1.23×10^{-6}A/ng/mL	[30]
2.	CNTs/[c]PDDA/Pd-Au	DPV	0.03	0.05–25	–	[31]
3.	[d]PEDOT/AuNPs/ITO	[i]CV	0.004	1–25	3.72 μA ng/mL	[32]
4.	SWCNTs[e]/Chitosan	DPV	0.003	0.01–100	–	[33]
5.	[f]CS-AuNPs/gold microelectrode	CV	0.12	0.2–2.0	72.3 μA	[34]
6.	[g]rGO/ITO	CV	0.12	0.125-1.5	68 μA	[35]
7.	GQDs-AuNPs/ITO	CV	0.008	0.1–3.0	382 μA ng^{-1} mL cm^{-2}	Present work

*[a] PTH-polythionine, [b] GCE-glassy carbon electrode, [c] PDDA-poly(diallyldimethylammoniumchloride),
[d] PEDOT-poly(3,4-ethylenedioxythiophene), [e] SWCNT-single walled carbon nanotubes, [f] CS-Chitosan
[g] rGO-Reduced graphene oxide, [h] DPV- Differential Pulse Voltammetry,
[i] CV- Cyclic Voltammetry

Reproducibility, stability and selectivity studies of bioelectrode

Along with the biosensing performance of the immunosensor, some important parameters such as reproducibility, stability, selectivity play a crucial role in the development of sensitive and stable biosensor. Reproducibility studies of BSA/anti-AFB1/GQDs-AuNPs/ITO immunosensor were carried out by CV technique on different working electrodes under a similar experimental condition with AFB1 antigen concentration (1.0 ng mL^{-1}). It is found that immunosensor shows good reproducibility with their negligible variation in current response (Fig. S7(a)). For six working electrodes, relative standard deviation (RSD) found to be 2.65% (mean value 0.0011 A). Low RSD value of fabricating immunosensor shows good precision.

Storage stability of fabricated immunosensor was determined by observing the change in current response of BSA/anti-AFB1/GQDs-AuNPs/ITO bioelectrode per week up to the consecutive 8 weeks under the similar experimental conditions. The results of this study show that the electrode signal retained 94% of its initial response up to the fourth week, and after that signal, response decreases significantly that indicates the denaturation of biomolecules. Further, immunoelectrode was stored in the refrigerator (4 °C) when not in use. Stability of the immunoelectrode attributed to the well-ordered uniformed assembly of GQDs-AuNPs (as shown in SEM image), covalent immobilization of antibodies AFB1, where AFB1 biomolecules attached strongly in an effective manner thereby it reduces the leaching problem of biomolecules from the sensor surface. Therefore, fabricated immunosensor offers the stability of bioelectrode up to 8 weeks with a significant decrement in the response signal.

As shown in Fig. S7(b), selectivity studies were carried out to determine the interference potential with another toxin as ochratoxin-A. The bioelectrode BSA/anti-AFB1/GQDs-AuNPs/ITO was tested against the AFB1 (0.2 ng mL^{-1}) and ochratoxin (0.2 ng mL^{-1}) in 1:1 ratio using CV technique. The insignificant change in the current signal is observed in Fig. S7(b), indicates insufficient interference taken place with another analyte. This study revealed that fabricated immunosensor is highly selective towards the analyte AFB1.

Conclusions

An electrochemical immunoassay is described for sensitive and selective detection of AFB1 using a composite of GQDs-AuNPs as a transducer. The chemical process was utilized to conjugate the GQDs and AuNPs using 2-ATP as a linker where carboxy groups of GQDs bind to the amino groups of crosslinker via conjugation of thiol binding to the AuNPs. The structure and morphology of composite GQDs-AuNPs examined by various spectroscopic techniques. Further, biomolecules of AFB1 covalently immobilized over the electrode surface of GQDs-AuNPs/ITO using EDC-NHS crosslinkers. To study the electrochemical properties, electrochemical techniques such as CV and EIS were applied results revealed that GQDs-AuNPs composite improved not only conductivity but also offered a large surface area and good biocompatibility for the immobilization of antibodies. The electrochemical sensing response of fabricated immunosensor was determined using CV technique resulted that current signal increases as by increasing the concentration of AFB1 in the range of 0.1–3.0 ng mL^{-1}, is highly specific, has good reproducibility, and acceptable stability. The practicability of fabricated immunosensor spiked (maize) samples were analyzed by CV technique which shows current response dependency on concentration of AFB1 in the range of AFB1 from 0.1 to 2.5 ng mL^{-1} and limit of detection of this sensor is 0.11 ng mL^{-1} which is lower than the maximum tolerance level for AFB1 in EU regulations. The method potentially can be utilized for detection of other mycotoxins such as ochratoxin, citrinin, etc. by using their respective antibodies.

Acknowledgments Authors are highly thankful to Director, CSIR-National Physical Laboratory, New Delhi, India, for providing the facilities. The authors are thankful to Prof. B. D. Malhotra, Delhi Technical University, for his valuable guidance. H.B. acknowledge to Dr. Ritu Srivastava for PL studies, Dr. Vikas Sharma for kind support and Mr. Jai S. Tawale for SEM studies.

Compliance with ethical standards The author(s) declare that they have no competing interests.

References

1. Wan L, Du C, Yang S (2017) Synthesis of graphene oxide/polybenzoxazine-based nitrogen-containing porous carbon nanocomposite for enhanced supercapacitor properties. Electrochim Acta 251:12–24
2. Rajender G, Giri PK (2016) Formation mechanism of graphene quantum dots and their edge state conversion probed by photoluminescence and Raman spectroscopy. J Mater Chem C 4(46):10852–10865
3. Martin A, Escarpa A (2014) Graphene: the cutting–edge interaction between chemistry and electrochemistry. Trends Anal Chem 56: 13–26
4. Mollarasouli F, Asadpour-Zeynali K, Campuzano S, Yáñez-Sedeño P, Pingarrón (2017) Non-enzymatic hydrogen peroxide sensor based on graphene quantum dots-chitosan/methylene blue hybrid nanostructures. Electrochim. Acta 246:303–314
5. Szabó T, Berkesi O, Forgó P, Josepovits K, Sanakis Y, Petridis D, Dékány I (2006) Evolution of surface functional groups in a series of progressively oxidized graphite oxides. Chem Mater 18(11): 2740–2749
6. Yang H, Liu W, Ma C, Zhang Y, Wang X, Yu J, Song X (2014) Gold–silver nanocomposite-functionalized graphene based electrochemiluminescence immunosensor using graphene quantum dots coated porous PtPd nanochains as labels. Electrochim Acta 123:470–476
7. Luo X, Morrin A, Killard AJ, Smyth MR (2006) Application of nanoparticles in electrochemical sensors and biosensors. Electroanalysis 18(4):319–326
8. Huang K-J, Niu D-J, Liu X, Wu Z-W, Fan Y, Chang Y-F, Wu Y-Y (2011) Direct electrochemistry of catalase at amine-functionalized graphene/gold nanoparticles composite film for hydrogen peroxide sensor. Electrochim Acta 56(7):2947–2953
9. Ju J, Chen W (2015) In situ growth of surfactant-free gold nanoparticles on nitrogen-doped graphene quantum dots for electrochemical detection of hydrogen peroxide in biological environments. Anal Chem 87(3):1903–1910
10. Li J, Qu J, Yang R, Qu L, Harrington d B (2016) A sensitive and selective electrochemical sensor based on graphene quantum dot/gold nanoparticle nanocomposite modified electrode for the determination of quercetin in biological samples. Electroanalysis 28(6): 1322–1330
11. Zhang Z, Li Y, Li P, Zhang Q, Zhang W, Hu X, Ding X (2014) Monoclonal antibody-quantum dots CdTe conjugate-based fluoroimmunoassay for the determination of aflatoxin B1 in peanuts. Food Chem 146:314–319
12. da Rocha MEB, Freire FCO, Maia FEF, Guedes MIF, Rondina D (2014) Mycotoxins and their effects on human and animal health. Food Control 36(1):159–165
13. Ji X, Song X, Li J, Bai Y, Yang W, Peng X (2007) Size control of gold nanocrystals in citrate reduction: the third role of citrate. J Am Chem Soc 129(45):13939–13948
14. Dong Y, Shao J, Chen C, Li H, Wang R, Chi Y, Lin X, Chen G (2012) Blue luminescent graphene quantum dots and graphene oxide prepared by tuning the carbonization degree of citric acid. Carbon 50(12):4738–4743
15. Bhardwaj H, Singh C, kumar Pandey M, Sumana G (2016) Star shaped zinc sulphide quantum dots self-assembled monolayers: preparation and applications in food toxin detection. Sens Actuators B Chem 231:624–633
16. Ma H, Sun J, Zhang Y, Bian C, Xia S, Zhen T (2016) Label-free immunosensor based on one-step electrodeposition of chitosan-gold nanoparticles biocompatible film on au microelectrode for determination of aflatoxin B1 in maize. Biosens Bioelectron 80: 222–229
17. Qian K, Sweeny BC, Johnston-Peck AC, Niu W, Graham JO, DuChene JS, Qiu J, Wang Y-C, Engelhard MH, Su D (2014) Surface plasmon-driven water reduction: gold nanoparticle size matters. J Am Chem Soc 136(28):9842–9845
18. Tang L, Ji R, Cao X, Lin J, Jiang H, Li X, Teng KS, Luk CM, Zeng S, Hao J (2012) Deep ultraviolet photoluminescence of water-soluble self-passivated graphene quantum dots. ACS Nano 6(6): 5102–5110
19. Lin B, Yan Y, Guo M, Cao Y, Yu Y, Zhang T, Huang Y, Wu D (2018) Modification-free carbon dots as turn-on fluorescence probe for detection of organophosphorus pesticides. Food Chem 245: 1176–1182
20. Srivastava S, Abraham S, Singh C, Ali MA, Srivastava A, Sumana G, Malhotra BD (2015) Protein conjugated carboxylated gold@ reduced graphene oxide for aflatoxin B 1 detection. RSC Adv 5(7):5406–5414
21. Dhyani H, Ali MA, Pandey MK, Malhotra BD, Sen P (2012) Electrophoretically deposited CdS quantum dots based electrode for biosensor application. J Mater Chem 22(11):4970–4976
22. Lin Y, Liu K, Wang C, Li L, Liu Y (2015) Electrochemical immunosensor for detection of epidermal growth factor reaching lower detection limit: toward oxidized glutathione as a more efficient blocking reagent for the antibody functionalized silver nanoparticles and antigen interaction. Anal Chem 87(16):8047–8051
23. Karimi-Maleh H, Tahernejad-Javazmi F, Ensafi AA, Moradi R, Mallakpour S, Beitollahi H (2014) A high sensitive biosensor based on FePt/CNTs nanocomposite/N-(4-hydroxyphenyl)-3, 5-dinitrobenzamide modified carbon paste electrode for simultaneous determination of glutathione and piroxicam. Biosens Bioelectron 60:1–7
24. Nor NM, Razak KA, Lockman Z (2017) Physical and electrochemical properties of iron oxide nanoparticles-modified electrode for amperometric glucose detection. Electrochim Acta 248:160–168
25. Teixeira S, Conlan RS, Guy O, Sales MGF (2014) Novel single-wall carbon nanotube screen-printed electrode as an immunosensor for human chorionic gonadotropin. Electrochim Acta 136:323–329
26. Randviir EP (2018) A cross examination of electron transfer rate constants for carbon screen-printed electrodes using electrochemical impedance spectroscopy and cyclic voltammetry. Electrochim Acta 286:179–186
27. Sharma A, Rao VK, Kamboj DV, Gaur R, Upadhyay S, Shaik M (2015) Relative efficiency of zinc sulfide (ZnS) quantum dots (QDs) based electrochemical and fluorescence immunoassay for the detection of staphylococcal enterotoxin B (SEB). Biotechnol Reports 6:129–136
28. Okuno J, Maehashi K, Kerman K, Takamura Y, Matsumoto K, Tamiya E (2007) Label-free immunosensor for prostate-specific antigen based on single-walled carbon nanotube array-modified microelectrodes. Biosens Bioelectron 22(9–10):2377–2381
29. Kaushik A, Solanki PR, Ansari AA, Ahmad S, Malhotra BD (2008) Chitosan–iron oxide nanobiocomposite based immunosensor for ochratoxin-a. Electrochem Commun 10(9):1364–1368

30. Owino J, Arotiba O, Hendricks N, Songa E, Jahed N, Waryo T, Ngece R, Baker P, Iwuoha E (2008) Electrochemical immunosensor based on polythionine/gold nanoparticles for the determination of aflatoxin B1. Sensors 8(12):8262–8274
31. Zhang S, Shen Y, Shen G, Wang S, Shen G, Yu R (2016) Electrochemical immunosensor based on Pd–au nanoparticles supported on functionalized PDDA-MWCNT nanocomposites for aflatoxin B1 detection. Anal Biochem 494:10–15
32. Sharma A, Kumar A, Khan R (2017) Electrochemical immunosensor based on poly (3, 4-ethylenedioxythiophene) modified with gold nanoparticle to detect aflatoxin B1. Mater Sci Eng C 76:802–809
33. Zhang X, Li C-R, Wang W-C, Xue J, Huang Y-L, Yang X-X, Tan B, Zhou X-P, Shao C, Ding S-J (2016) A novel electrochemical immunosensor for highly sensitive detection of aflatoxin B1 in corn using single-walled carbon nanotubes/chitosan. Food Chem 192: 197–202
34. Ma H, Sun J, Zhang Y, SJBej X (2016) Disposable amperometric immunosensor for simple and sensitive determination of aflatoxin B1 in wheat. Biochem Eng J 115:38–46
35. Srivastava S, Kumar V, Ali MA, Solanki PR, Srivastava A, Sumana G, Saxena PS, Joshi AG, Malhotra B (2013) Electrophoretically deposited reduced graphene oxide platform for food toxin detection. Nanoscale 5(7):3043–3051